


Article

# Aerodynamic Interaction Minimization in Coaxial Multirotors via Optimized Control Allocation

Andrea Berra <sup>1,\*</sup>, Miguel Ángel Trujillo Soto <sup>1</sup> and Guillermo Heredia <sup>2</sup>

<sup>1</sup> CATEC (Advanced Center for Aerospace Technologies), C/ Wilbur y Orville Wright 19, La Rinconada, 41309 Seville, Spain; matrujillo@catec.aero

<sup>2</sup> GRVC Robotics Lab, Escuela Técnica Superior de Ingeniería, Universidad de Sevilla, 41092 Seville, Spain; guiller@us.es

\* Correspondence: aberra@catec.aero

**Abstract:** Coaxial multirotors, characterized by overlapping rotors, represent a common solution to increasing payload capacity while maintaining a compact platform size. However, the overlap between motors generates airflow disturbances that, if not taken into account properly, may decrease the system's overall performance. In this paper, aerodynamic interactions for coaxial multirotors are analyzed and characterized. Two rotor models are introduced, which account for the aerodynamic interaction between the upper and the lower rotor. Each model is accompanied by its corresponding mixer design and analyzed with respect to the state-of-the-art mixer solution for classical multirotor systems. The proposed approaches are tested through rotor stand experiments, simulations, and implementation on an actual coaxial platform. The results demonstrate the effectiveness of these models in mitigating the adverse aerodynamic effects, thereby improving the performance and efficiency of coaxial multirotor systems.

**Keywords:** aerodynamics; coaxial interaction; control allocation; multirotor



**Citation:** Berra, A.; Trujillo Soto, M.Á.; Heredia, G. Aerodynamic Interaction Minimization in Coaxial Multirotors via Optimized Control Allocation. *Drones* **2024**, *8*, 446. <https://doi.org/10.3390/drones8090446>

Academic Editors: Mostafa Hassanalain, Ni Li, Ban Wang and Shuhui Bu

Received: 17 July 2024

Revised: 13 August 2024

Accepted: 28 August 2024

Published: 30 August 2024



**Copyright:** © 2024 by the authors. Licensee MDPI, Basel, Switzerland. This article is an open access article distributed under the terms and conditions of the Creative Commons Attribution (CC BY) license (<https://creativecommons.org/licenses/by/4.0/>).

## 1. Introduction

Unmanned aerial vehicles (UAVs) have attracted a lot of interest recently from a variety of industry sectors due to their ability to carry out crucial tasks in hazardous environments, such as inspection tasks and search and rescue missions, among others. To address evolving demands, UAV platforms have undergone considerable evolution from the beginning, expanding in both size and payload capacity. Departing from the first quadrotor designs, a diverse variety of configurations has emerged to increase safety and robustness during operations [1]. Among these configurations, coaxial multirotors have been tested in recent years [2–4], particularly for the possibility of carrying high payloads in a compact footprint, since using coaxial rotors allows for a significant increase in power without the need to increase the size of the platform. However, the presence of rotors located on top of each other generates aerodynamic flux among the two, which can compromise the control and stability of the platforms if not properly considered in the mixing strategy. Motivated by the necessity of advancing the precise control of coaxial multirotors, this paper presents a novel coaxial rotor model and control allocation aiming to model and minimize coaxial aerodynamic interactions between coaxial rotors.

### 1.1. Related Work

In the past few decades, control allocation has been extensively researched [5] for UAVs. Various methodologies have been developed to robustly and effectively compute desired rotor velocities, such as the optimal control allocation method [6,7], quadratic programming-based methods [8,9] and neural network-based techniques [10]. The methodologies presented in [5–10] primarily focus on investigating novel techniques to tackle

control allocation challenges, particularly concerning issues like singularity, rotor saturation, and optimality of the solution. However, little attention has been directed towards the study of the aerodynamic complexities generated by rotor propellers. Indeed the majority of the allocation methods rely on the standard constant rotor model derived in [11], which defines that the thrust and torque produced by a single rotor are proportional to its velocity squared. This rotor model has been proven to be accurate in ideal conditions and with no rotor overlap, whereas for coaxial rotors the proximity of the two rotors generates aerodynamic flux, which causes additional thrust and torque components, as analyzed in [12–16], making the standard model not valid anymore. In particular, in [13] a study on aerodynamic interaction for counter-rotating coaxial rotor is proposed, while in [14] a numerical analysis of interaction effect at different rotor spacing is presented; finally, in [15] the aerodynamic performance of a coaxial hexacopter is studied for different rotor spacing. The analysis indicates that the aerodynamic performance is affected by the proximity of two rotors, both in thrust and torque. From a control perspective, in the design of the control structure for coaxial multirotors, aerodynamic effects due to rotor proximity are often neglected [17–20] or treated simplistically. One common choice in this regard is the inclusion of a constant penalization gain in the control allocation design to consider the thrust loss due to rotor proximity [21–23]. However, this conventional approach fails to capture the complex and nonlinear interactions between lower and upper rotors by just considering a linear model. Another common approach to compensate for coaxial thrust loss is to increase the diameter of the lower rotor propeller with respect to the upper one to increase its thrust and thus compensate for thrust loss, as mentioned in [24]. However, this method has several disadvantages. Increasing the lower rotor size can lead to additional weight and structural complexity, as well as the addition of aerodynamic drag and noise, which overall decrease the efficiency of the system. Other solutions present the integration of more complex thrust models in control allocation structure [10,25–28]. In [10], a neural-network-based mixing strategy proposes to compensate for nonlinear aerodynamics effects generated in multirotors. A similar approach is adopted in [25], specifically targeting the compensation of coaxial aerodynamics effects. Although neural network-based solutions are generally capable of accurately modeling highly nonlinear systems, they impose a substantial computational burden. This increased computational demand makes it very challenging to deploy such solutions in real systems, given the high frequencies typically required by mixers in multirotor systems. In [26], quadratic polynomials are used to model rotor thrust and torque based on input speed. However, the nonlinear models are not explicitly integrated into the mixing strategy. In [27], a similar approach is adopted, a nonlinear polynomial is utilized to estimate the total thrust and torque for a coaxial rotor unit of an octacopter. Despite being evaluated on a real system, the approach presented relies on a thrust and torque color map to compute the rotor velocities from coaxial thrust, which is limited by the color map resolution and introduces uncertainty caused by the interpolation of the colormap. In [28], an optimal efficiency-based solution is developed and applied to a multirotor prototype. While this approach provides valuable insights into the efficiency of the coaxial platform, it merely focuses on the overall efficiency in the development of the coaxial mixer rather than on its accuracy for thrust and torque.

Overall, the studies mentioned propose solutions that are either computationally demanding, such as neural networks, or lack precision due to multiple interpolation steps or prioritizing efficiency without adequately evaluating the accuracy of thrust and torque.

### 1.2. Contributions

In this work, two coaxial mixers to minimize aerodynamic interaction in coaxial multirotors are designed. Unlike other solutions, the proposed model distinguishes between the thrust contributions of the upper and lower rotors and it is defined as a priori unknown polynomial order, whose order is determined through the identification process. While existing literature frequently presents solutions that either rely on highly computationally intensive models or empirical polynomial equations, the mixers developed in this work

from the rotor model generate analytical solutions for control allocation problems. Further, the proposed mixers are designed for rapid integration with standard allocation structures. Consequently, the main contributions of the presented works are (i) the development of an advanced coaxial rotor model that incorporates the effects of coaxial aerodynamic interaction, (ii) the integration of a coaxial aerodynamic effect into the allocation control problem, (iii) the adoption of the LASSO identification method for coaxial rotor model identification.

## 2. Coaxial Rotor

In order to effectively compensate for the interaction between upper and lower rotor velocities in determining overall force and torque, this section is devoted to the introduction of a nonlinear model for a generic coaxial rotor unit, the Coaxial Rotor Model (CRM). Additionally, the model will be detailed, along with the validation procedure conducted on a typical rotor test stand.

### 2.1. Model

A single coaxial unit, composed of a lower rotor  $(\cdot)_l$  and an upper rotor  $(\cdot)_u$ , is considered. The two rotors are aligned vertically, separated from each other by a distance of  $h$ , and equipped with the same propeller geometry. Further, it is assumed that the rotor speed of the two can be controlled separately. Then, building on the second-order polynomial model for coaxial thrust and torque proposed in [27], the approach developed in this paper extends the model to include higher polynomial degrees and separately models the thrust and torque for the upper and lower rotors. Consequently, upper and lower thrust and torque are introduced:

$$f_u = \gamma_u^f(u_u) \tag{1a}$$

$$\tau_u = \gamma_u^\tau(u_u) \tag{1b}$$

$$f_l = \gamma_l^f(u_l, u_u) \tag{1c}$$

$$\tau_l = \gamma_l^\tau(u_l, u_u) \tag{1d}$$

where  $\gamma_u^f, \gamma_u^\tau$  are polynomials of degree  $N$ ,  $\gamma_l^f, \gamma_l^\tau$  are polynomial surfaces of order  $P$ ,  $u_l, u_u$  are the normalized velocities for the upper and lower rotor velocities, and  $f_u, \tau_u, f_l, \tau_l$  represent, respectively, upper thrust, upper torque, lower thrust and lower torque. The upper rotor is considered dependent merely on its velocity, assuming a negligible effect of the upper rotor with respect to the lower one on the overall thrust and torque, as demonstrated in [14,29]. On the other hand, the influence of upper rotor flux with respect to the lower one has been considered in the model (Equation (1c,d)) since it always operates in the altered flow of the other. This provides the need to consider the two velocities for both the lower thrust and torque models. Considering this, the right side of Equation (1) can be expressed as:

$$\left\{ \begin{array}{l} \gamma_u^f = \sum_{i=N}^{i=0} (p_i u_u^{N-i}) \\ \gamma_u^\tau = \sum_{i=N}^{i=0} (q_i u_u^{N-i}) \\ \gamma_l^f = \sum_{i=N}^{i=0} \left( \sum_{j=M}^{j=0} p_k u_u^{N-i} u_l^{M-j} \right) \\ \gamma_l^\tau = \sum_{i=N}^{i=0} \left( \sum_{j=M}^{j=0} q_k u_u^{N-i} u_l^{M-j} \right) \end{array} \right. \tag{2}$$

where  $N$  is the maximum front rotor velocity exponent,  $M$  the maximum lower rotor velocity exponent such that  $P = M * N$ , and  $p_k$  and  $q_k$  are the  $p$ -th coefficients for, respectively,

thrust and torque (with  $k = 1, \dots, M * N$ ). Integrating Equation (2) into Equation (1c) and Equation (1), the overall thrust and torque for the two rotors is defined in a matrix form:

$$\begin{bmatrix} f_l \\ \tau_l \end{bmatrix} = \begin{bmatrix} \theta_l^f \\ \theta_l^\tau \end{bmatrix} \varphi, \quad \begin{bmatrix} f_u \\ \tau_u \end{bmatrix} = \begin{bmatrix} \theta_u^f \\ \theta_u^\tau \end{bmatrix} \varphi \quad (3)$$

where  $\theta_{u,l}^f, \theta_{u,l}^\tau \in \mathbb{R}^{1 \times P}$  are the unknown coefficient matrices, and  $\varphi \in \mathbb{R}^{P \times 1}$  is the velocity regressor matrix. It is important to notice that the coaxial model presented is also influenced by the blade geometry and the coaxial distance  $h$  between the two rotors. In particular, as shown in [11], the rotor thrust and torque parameters for a single rotor, are computed based on the performance of the motor and the geometrical shape of the blade. Further, the influence of coaxial distance on the thrust and torque performance of the rotors has been studied in [30,31]. The performance of the upper rotor results in being negligibly affected by the proximity of the lower rotor due to its operation in the upstream. However, the thrust and torque of the lower rotor result in being significantly dependent on the coaxial distance, with closer proximity to the upper rotor resulting in greater thrust loss in the lower rotor. This makes its thrust and torque coefficient (Equation (1)) dependent on the coaxial distance. These insights directly impact the model presented in Equation (1). In particular, increasing the coaxial distance  $h$  results in an increase in the overall lower rotor thrust and torque due to the decrease in the penalization terms related to upper rotor velocities. On the other hand, a decrease in  $h$  leads to a decrease in the lower rotor thrust and torque as a consequence of the increased penalization due to the upper rotor's flux. Modifications in the distance  $h$ , as reported in [30], do not affect the coefficients for the upper rotor's thrust and torque. Overall, changes in the propeller geometry would necessitate a reevaluation of the coefficient values for both the upper and lower rotors [11], while a change in the coaxial distance would imply a difference in the value of lower rotor coefficients. However, the model presented in Equation (1) has been presented not assuming specific rotor or propeller performance, relying instead on the aerodynamic interaction between the two rotors, which is caused by the coaxial configuration.

## 2.2. Identification Method

For the estimation of the unknown parameter vector of Equation (3), a Least Absolute Shrinkage and Selection Operator (LASSO) method is adopted. LASSO is an identification technique introduced in [32] that allows computing unknown constant parameters that can best fit the proposed model. In contrast to the most used Least Square (LS) technique, LASSO minimizes the residual between the data and the model with a penalization on the vector norm. This allows us to overcome over-fitting problems that may arise with classical techniques such as LS [33] and constrain the complexity of the model. In particular, for the model presented in Equation (1), a NonLinear LASSO method (NL-LASSO) is adopted for the identification of four  $\theta$  vectors of Equation (3). Following the structure introduced in [34], the NL-LASSO problem for the upper and lower rotors becomes:

$$\begin{aligned} \hat{\theta}_i^f &= \underset{\theta_i^f}{\operatorname{argmin}} \|\tilde{f}_i - \varphi(\tilde{u}_i, \tilde{u}_u)\theta_i^f\|_2^2 + \lambda^f \|\theta_i^f\|_1 \\ \hat{\theta}_i^\tau &= \underset{\theta_i^\tau}{\operatorname{argmin}} \|\tilde{\tau}_i - \varphi(\tilde{u}_i, \tilde{u}_u)\theta_i^\tau\|_2^2 + \lambda^\tau \|\theta_i^\tau\|_1 \\ &\text{with } i = \{u, l\} \end{aligned} \quad (4)$$

where  $\lambda^{f,\tau}$  are regularization terms,  $\|\cdot\|_2$  indicates the  $l_2$ -norm,  $\|\cdot\|_1$  the  $l_1$ -norm,  $(\tilde{\cdot})$  indicates the measured quantities while  $(\hat{\cdot})$  the estimated ones.  $(\cdot)_i$  represents the quantity related to the upper rotor  $u$  or lower rotor  $l$ . Equation (4) can be then formulated as quadratic programming optimization problems and efficiently solved using a standard

optimizer, providing the optimal coefficients to fit the thrust and momentum of the coaxial rotor unit.

### 3. Coaxial Rotor Experiments and Analysis

This section is devoted to the experimental part of the coaxial rotor model. In particular, two main aspects have been analyzed: the identification of unknown coefficients for the rotor model and the analysis of the model obtained with respect to the identification tolerance and efficiency.

#### 3.1. Parameter Identification

For the identification of the parameters of the model developed in Section 2, a series of tests have been conducted using a rotor testing platform. The platform allows sending *ESC* signals for both rotors simultaneously and measures various quantities, including rotor thrust, torque, and velocities. All the tests have been conducted in the center of a large room to avoid air vortex and with similar light and temperature conditions to minimize the influence of environmental factors, such as humidity and air density throughout the tests. For the tests, two rotors *KDE5215XF-220* are located one in front of each other in the testbed, as highlighted in Figure 1, and the two rotors are equipped with triple-propeller blades  $18.5'' \times 6.3$ . The rotor distance in the thrust stand is set equal to the actual coaxial distance on the testing platform (15 cm) to correlate the measurements collected from the thrust stand with those obtained from the testing prototype, as further explained in Section 5.1. The tests are performed by sending a PWM ramp signal on both rotors simultaneously. To map the whole set of possible combinations of PWMs between the two rotors, for each PWM value sent to the front rotor, a ramp (from 0% to 90% throttle) is given to the back rotor. This gives a dataset of 121 for the identification process. The dataset is then divided into two subsets: a training set and a test set. Specifically, 70% of the samples are allocated to the training set, while the remaining ones are dedicated to the test set. The data division is performed using the Holdout method to ensure a robust evaluation of the identified model.

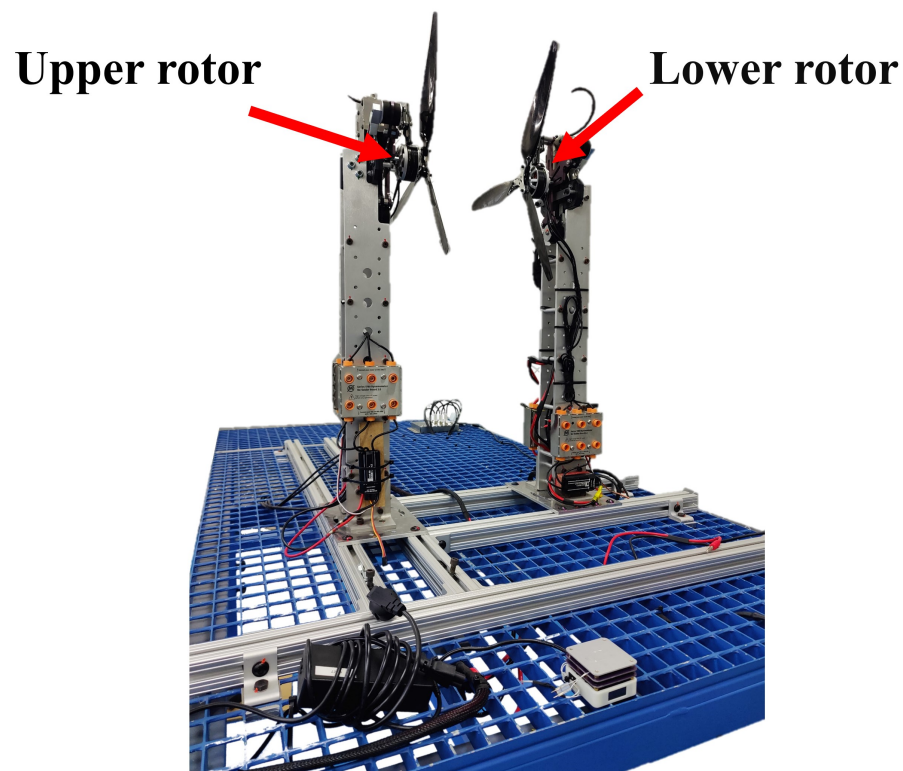


**Figure 1.** Thrust testbed in a coaxial configuration.

The collected data from experiments are then used for the estimation of unknown coefficients of Equation (3) by applying the NL-LASSO introduced in Equation (4). The NL-LASSO algorithm implementation was realized using the CVX optimization toolbox with the MOSEK solver (<https://cvxr.com/>, accessed on 10 August 2024). The tolerance for the thrust optimization routine has been set to  $\epsilon_T$  to  $2N$  and the tolerance for torque optimization routine  $\epsilon_M$  to 0.05 Nm to prevent overfitting. To avoid an excessive increase in the number of estimated coefficients, the maximum exponent for both the upper and lower rotor is constrained to two ( $M = N = 2$ ). Analyzing the estimated coefficients provided in Table 1 for the upper rotor, it becomes evident that the primary contributions to the overall thrust and torque of the two rotors come from the square of velocities and the corresponding linear velocity terms, while the other contributions are considered negligible.

**Table 1.** Values of estimated coefficients for upper and lower rotors with LASSO. All rotor velocity values are normalized.

Lower rotor coefficients					
Thrust	$u_l^2 u_u^2$	$u_l u_u^2$	$u_l^2 u_u$	$u_l u_u$	$u_u^2$
	2.755	$2.166 \times 10^{-9}$	$1.047 \times 10^{-9}$	-2.547	-37.502
Torque	$u_l^2$	$u_l$	<i>const</i>		
	64.721	12.402	0.801		
Torque	$u_l^2 u_u^2$	$u_l u_u^2$	$u_l^2 u_u$	$u_l u_u$	$u_u^2$
	$1.685 \times 10^{-10}$	$-9.398 \times 10^{-12}$	0.307	$4.991 \times 10^{-10}$	-0.695
Torque	$u_l^2$	$u_l$	<i>const</i>		
	1.466	0.573	$2.987 \times 10^{-10}$		
Upper rotor coefficients					
Thrust	$u_u^2$	$u_u$	<i>const</i>		
	55.9517	22.4464	$1.4629 \times 10^{-8}$		
Torque	$u_u^2$	$u_u$	<i>const</i>		
	1.2437	0.7155	$2.1277 \times 10^{-8}$		

This finding is consistent with [7,35], where it has been found that a linear plus a squared velocity provides a better fit with respect to the conventional approach [11] data for a single rotor. This behavior appears to persist for the upper rotor in a coaxial configuration, indicating that the presence of the lower rotor minimally influences the upper rotor. On the other hand, observing the estimated coefficients for the lower rotor, the standard thrust model appears not to be a good model choice for coaxial configuration. This concept is further explored in Figure 2, which compares the rotor thrust and torque for each rotor with its squared velocities. The plots reveal a general deviation from the linear model for the lower rotors, with significant uncertainty observed in both thrust and torque. It is particularly evident at low lower rotor velocities, where the flow from the upper rotors appears to exert a significant influence on the lower rotor.

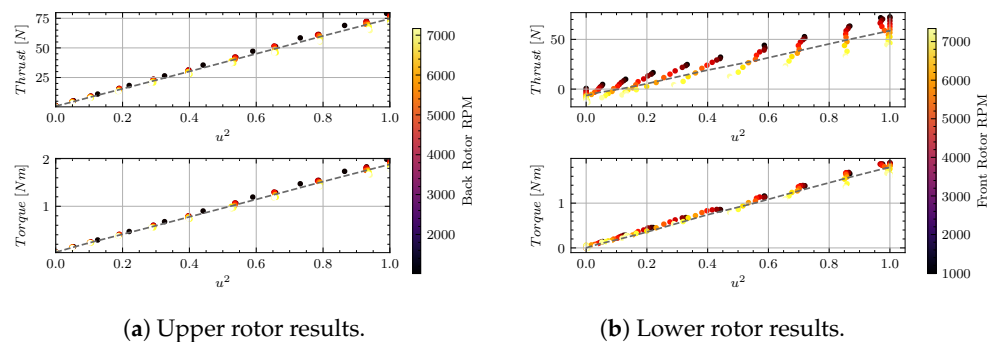


**Figure 2.** Variation of linear correlation between thrust (torque) and rotor velocities squared with changing velocities of the opposing coaxial rotor. The grey dotted line underlines the linear trend.

With the estimated quantities, an evaluation of the quality of the introduced model has been performed. Table 2 presents the analysis of the model performance considering some common indicators for the coaxial thrust and torque. A comparison between the presented *Coaxial Rotor Model* and various models adopted in the literature is proposed, demonstrating a significant reduction in both thrust and torque with the presented model relative to the most commonly used models.

**Table 2.** Evaluation of Coaxial Rotor Model (CRM) and Relaxed Coaxial Rotor Model (R-CRM) with respect to coaxial thrust ( $f_{coaxial} = f_u + f_l$ ) and coaxial torque ( $\tau_{coaxial} = \tau_u + \tau_l$ ) and comparison with different models: Single Rotor Model (SRM) [11], Constant Penalization Coaxial Model (CPCM) from [21].

	Coaxial Thrust			Coaxial Torque		
	RMSE	NRMSE	R-Value	RMSE	NRMSE	R-Value
CRM	1.1614	0.0106	0.9997	0.0241	0.0072	0.9998
R-CRM	4.2116	0.0385	0.9956	0.1016	0.0305	0.9971
SRM [11]	12.8323	0.0775	0.9718	0.2029	0.0523	0.9911
CPCM [21]	12.7638	0.0771	0.9721	0.2029	0.0523	0.9911

### 3.2. Tolerance Analysis

One of the main aspects of the LASSO approach for the estimation of unknown parameters is the proper selection of tolerance values  $\eta$ ; a too-small tolerance may lead to overfitting problems while a too-large value may result in a bad fit of the data. Values chosen in Section 2 represent a good compromise among the feasible solutions for the solver because they guarantee a good fit while reducing the number of parameters initially chosen. The validation of the developed model is further analyzed by performing the sensitivity analysis on the estimated coefficients (Table 1) with respect to the chosen thrust and torque tolerance. The results are presented in Figure 3.

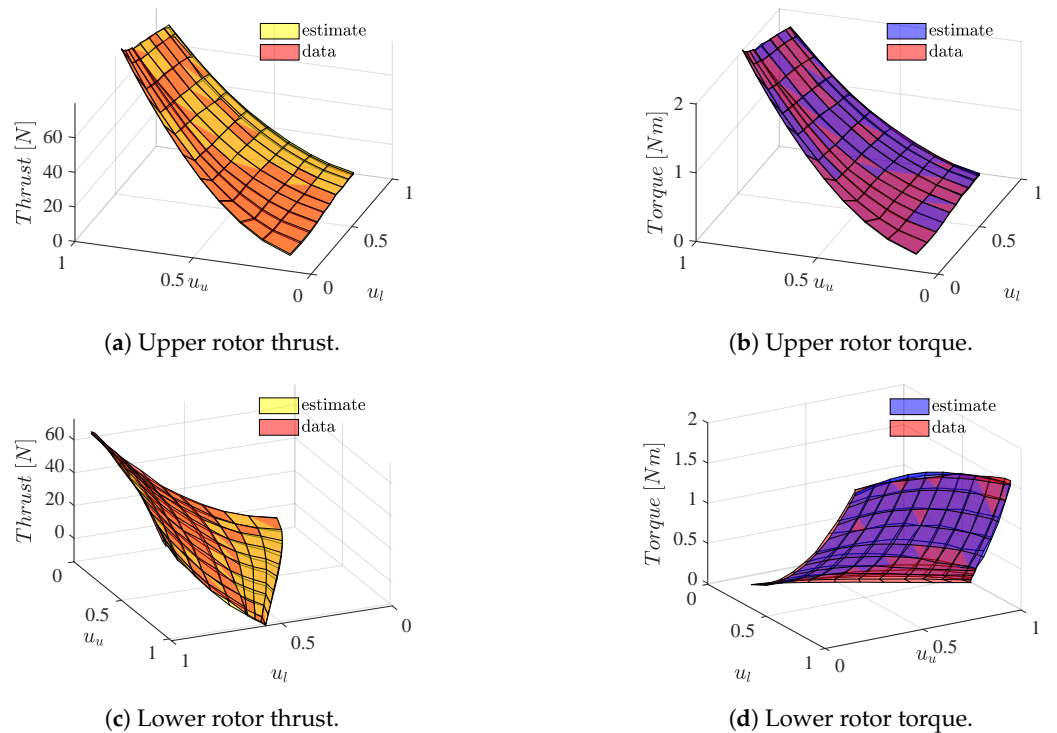


**Figure 3.** Thrust and torque maps for upper and lower rotor velocities, comparison between data (red) and model (yellow and blue).

In the test, a LASSO optimization routine for the upper and the lower rotor is performed with a tolerance relaxation up to 0.1 Nm for the torque and 10 N for the thrust.

The results obtained in Figure 4 provide no remarkable findings for the upper rotor. However, for the lower rotor, a notable transition to a quadratic model is observed when the tolerance exceeds 10 N for thrust and 0.2 Nm for torque. Under this condition, the new model, *Reduced Coaxial Rotor Model* (R-CRM), still provides lower accuracy with respect to the CRM of Section 2, but still a better one compared with the standard rotor model (see Table 1). Overall, it has been observed that an increase in the tolerance value in the LASSO routine results in a decrease in the model accuracy, but with a decrease in the complexity of the model generated. On the other hand, a decrease in the LASSO tolerance value results in an increase in the accuracy due to an increase in the complexity of the model, as summarized in Table 3. The obtained new model, R-CRM, presents the possibility of directly adjusting the control allocation matrix for a no-coaxial multirotor with coaxial contribution since it only presents a quadratic relation with respect to both rotor velocities.

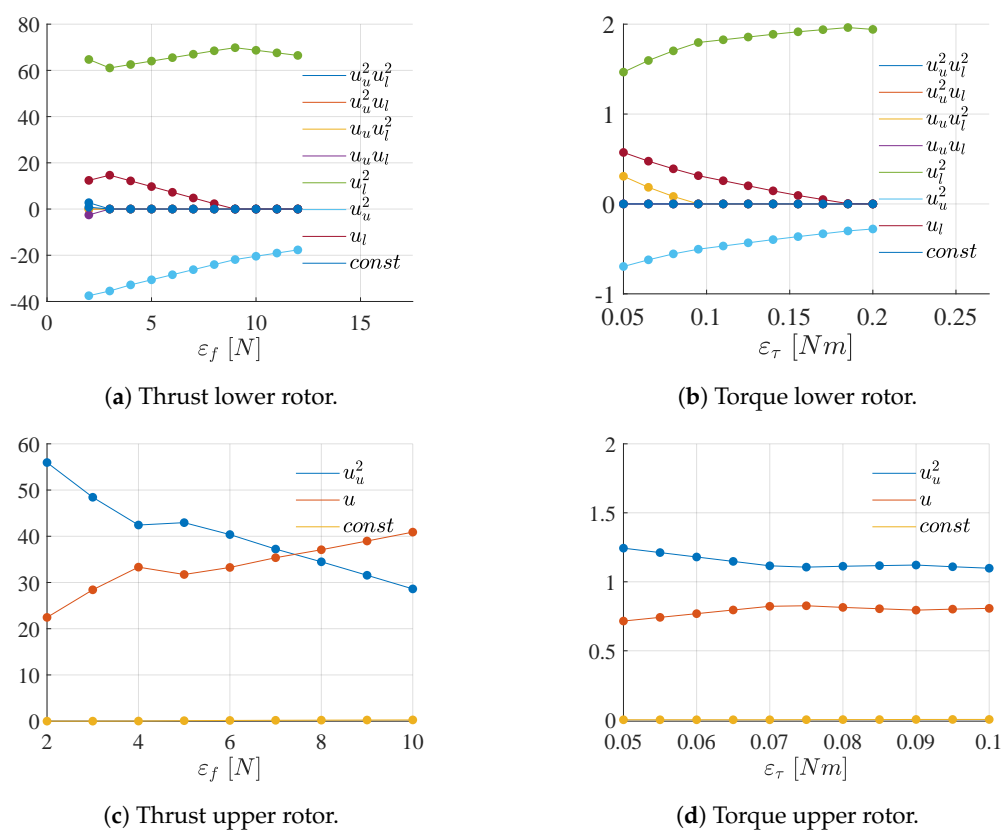


**Figure 4.** Variation of estimated thrust and torque parameters for upper and lower rotors with respect to corresponding LASSO tolerance.

**Table 3.** Comparison of the proposed models (CRM and R-CRM) with respect to the accuracy, LASSO tolerance, and model complexity. The arrows indicate the relative performance of each model: ↑ denotes improvement, and ↓ denotes a decrease in the respective metric.

	Accuracy	Tolerance	Model Complexity
CRM	↑	↓	↑
R-CRM	↑	↓	↑

### 3.3. Efficiency

Efficiency is a crucial factor in evaluating multirotor systems, as an efficient system can extend flight time and prevent potential motor overheating. This consideration is significant for coaxial multirotors, where aerodynamic interactions between the rotors impact overall



system efficiency. In this section, the efficiency of the coaxial rotor velocities generated by the proposed model is evaluated in comparison with the standard configuration. The motor electric efficiency  $\eta_{motor}$  and the propeller efficiency  $\eta_{propeller}$  for a coaxial rotor can be defined as:

$$\eta_{prop} = \frac{T_{coax}}{\tau_u \omega_u + \tau_l \omega_l} \quad (5a)$$

$$\eta_{motor} = \frac{\tau_u \omega_u + \tau_l \omega_l}{V_u I_u + V_l I_l} \quad (5b)$$

where  $T_{coax}$  represents the total thrust of coaxial rotors,  $\tau$  the rotor torque,  $\omega$  the rotor velocity,  $V$  the voltage and  $I$  the current. The overall efficiency can be defined as the product of the mechanical and electrical efficiencies  $\eta_{coax} = \eta_{prop} \eta_{motor}$ . As examined in [28], the efficiency of coaxial rotors exhibits an upper bound for the whole thrust domain, defined as  $\eta^*$ . However,  $\eta^*$  is generally not reached by rotating the two propellers at the same speed, which is the case when adopting a standard mixer. These observations align with the findings illustrated in Figure 5, where the efficiency of the presented model is evaluated. In particular, a set of coaxial thrusts is defined and applied to Equation (1a–d) to compute motor speed and torque and thus the propeller efficiency (Figure 5a). The efficiency is then compared with the case of equal rotor velocities of standard mixers. The results show an average increment of  $\Delta\eta_{prop} = 0.0274N/W$  in favor of the coaxial model velocities. The electrical efficiency is then calculated by mapping upper and lower currents to their respective rotor speed. Given motor efficiency and propeller efficiency, the overall efficiency is found by multiplying the two. The data displayed in Figure 5b highlight an average increment of  $\Delta\eta_{motor} = 0.0296N/W$  as well for the overall efficiency. Overall, the results indicate that the rotor velocities generated by the presented coaxial model exhibit better efficiency compared to the standard mixer where both rotors operate at identical speeds.

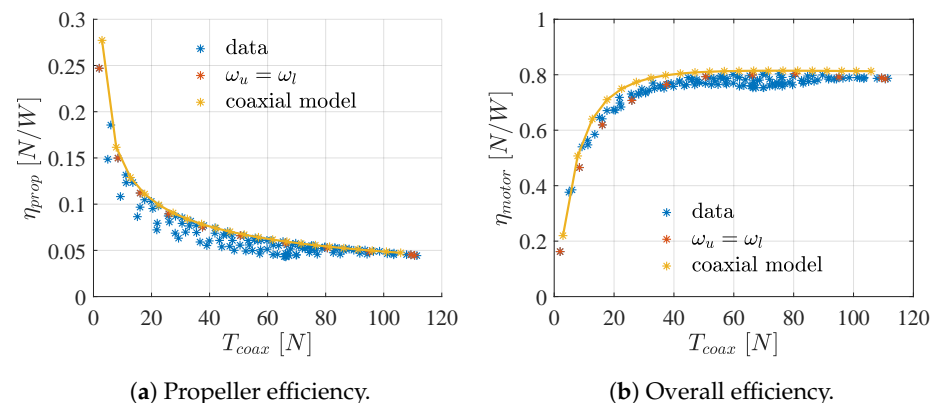


**Figure 5.** Coaxial rotor efficiencies for coaxial thrust: comparison between measured efficiency (blue), efficiency computed from the coaxial model (yellow), and efficiency at equal rotor speed (orange).

#### 4. Coaxial Control Allocation Strategies

The control allocation problem for coaxial underactuated multirotors consists of computing optimal upper rotor velocities  $u_u$  and lower rotor velocities  $u_l$  so that the desired forces and moments are achieved. Starting from the coaxial rotor models developed in Section 2, two coaxial mixers are developed in this section to compute optimal rotor velocities for coaxial multirotors.

##### 4.1. Reduced Coaxial Mixer

In Section 3.2, it has been demonstrated that the coaxial rotor model presents quadratic behavior in the case of tolerance relaxation. Under these conditions, from Equations (1a–d)

and (2), rotor forces and torques for an upper rotor and its corresponding lower one can be expressed:

$$\begin{cases} f_u = p_{0,u}u_u^2 \\ f_l = p_{0,l}u_l^2 + p_{1,l}u_u^2 \\ \tau_u = q_{0,u}u_u^2 \\ \tau_l = q_{0,l}u_l^2 + q_{1,l}u_u^2 \end{cases} \text{ with } p_0, q_0 > 0, p_1, q_1 < 0 \tag{6}$$

From Equation (6), the static control allocation matrix for a coaxial multirotor with Q upper rotors and S lower rotors is then defined as:

$$A = \begin{bmatrix} \tilde{p}_{u_1} & \dots & \tilde{p}_{u_Q} & p_{l_1} & \dots & p_{l_S} \\ ls_{\gamma_{u_1}}\tilde{p}_{u_1} & \dots & ls_{\gamma_{u_Q}}\tilde{p}_{u_Q} & ls_{\gamma_{u_1}}p_{l_1} & \dots & ls_{\gamma_{u_S}}p_{l_S} \\ -lc_{\gamma_{u_1}}\tilde{p}_{u_1} & \dots & -lc_{\gamma_{u_Q}}\tilde{p}_{u_Q} & -lc_{\gamma_{u_1}}p_{l_1} & \dots & -lc_{\gamma_{u_S}}p_{l_S} \\ \eta_{u_1}\tilde{q}_{u_1} & \dots & \eta_{u_Q}\tilde{q}_{u_Q} & \eta_{u_1}q_{l_1} & \dots & \eta_{u_S}q_{l_S} \end{bmatrix} \tag{7}$$

where  $l$  is the distance from the CoM of the platform to the rotor center,  $\eta_i$  is the  $i$ -th rotor rotation (1 for clockwise rotation,  $-1$  for counter-clockwise rotation),  $\gamma_i$  is the  $i$ -th rotors angle with respect to  $x_B$ , and  $(f, \tau_x, \tau_y, \tau_z)$  are, respectively, the overall thrust and the torques in the body fixed frames.  $\tilde{p}_u$  is defined as the difference between the upper rotor coefficient and the coaxial penalization term in the corresponding lower rotor:  $\tilde{p}_{u_i} = p_{0,u_i} + p_{1,l_i}$ . For simplicity  $p_{0,l} = p_l, q_{0,l} = q_l$ . From Equation (6), the desired velocities are obtained for the computed trust and torque. The introduction of penalization terms  $p_{1,l}, q_{1,l}$  into the mixer structure, leads to a separation between upper and lower rotor velocities in the computation process. Specifically, compared to a standard mixer, lower rotor velocities are higher relative to their corresponding upper ones. This adjustment results in improved overall system control, as analyzed in more detail in Section 5.3. Applying the Moore pseudoinverse lower and upper rotor velocities can be obtained from the desired body torques and the overall thrust.

#### 4.2. Coaxial Mixer

Following CRM introduced in Section 2, the sum of body forces and body torques for a coaxial multirotor with Q upper rotors and S lower rotors is defined as:

$$\begin{cases} f = \sum_{i=1}^{i=Q} f_{u_i} + \sum_{i=1}^{i=S} f_{l_i} \\ \tau_x = \sum_{i=1}^{i=Q} ls_{\gamma_i}f_{i_u} + \sum_{i=1}^{i=S} ls_{\gamma_i}f_{i_l} \\ \tau_y = -\sum_{i=1}^{i=Q} lc_{\gamma_i}f_{i_u} - \sum_{i=1}^{i=S} lc_{\gamma_i}f_{i_l} \\ \tau_z = \sum_{i=1}^{i=Q} \eta_i\tau_{i_u} + \sum_{i=1}^{i=S} \eta_i\tau_{i_l} \end{cases} \tag{8}$$

Equation (8) can be written in the more compact matrix form as:

$$\mu = A \begin{bmatrix} f \\ \tau \end{bmatrix} \tag{9}$$

where  $A \in R^{4,2(Q+S)}$  is the static control allocation matrix,  $f, \tau \in R^{(Q+S)}$  are, respectively, the thrust and torque vector composed of the upper and lower rotor thrust and rotor torques:

$$f = [f_{1_u}, \dots, f_{Q_u}, f_{1_l}, \dots, f_{S_l}] \tag{10}$$

$$\tau = [\tau_{1_u}, \dots, \tau_{Q_u}, \tau_{1_l}, \dots, \tau_{S_l}] \tag{11}$$

The desired rotor thrust and torque are then computed by computing the Moore–Penrose inverse of matrix  $A$ :

$$\begin{bmatrix} f^d \\ \tau^d \end{bmatrix} = A^+ \mu \tag{12}$$

where  $A^+$  is the pseudoinverse of matrix  $A$ . From Equations (1a–d), (8) and (12), the relationship between the desired forces and torque and rotor velocities is found:

$$\begin{bmatrix} f_u^d \\ \tau_u^d \\ f_l^d \\ \tau_l^d \end{bmatrix} = \begin{bmatrix} \Gamma_u^f(U_u) \\ \Gamma_u^\tau(U_u) \\ \Gamma_l^f(U_u, U_l) \\ \Gamma_l^\tau(U_u, U_l) \end{bmatrix} \tag{13}$$

where  $f_u^d, f_l^d, \tau_u^d, \tau_l^d$  are, respectively, the desired force and torque of upper and lower rotors,  $\Gamma_u^{(f,\tau)} \in R^Q, \Gamma_l^{(f,\tau)} \in R^S$  are the vectors for each rotor in the CRM model (Section 2),  $U_u \in R^Q$  and  $U_l \in R^S$  are the vectors containing the upper and lower rotor velocities. From Equation (13), the upper rotor velocities vector is then computed by solving  $Q$  polynomial of order  $N$ . After computing  $U_u$ , the lower part of Equation (13) becomes:

$$\begin{bmatrix} f_l^d \\ \tau_l^d \end{bmatrix} = \Theta_l \begin{bmatrix} \varphi_1(\bar{u}_1)^T \\ \dots \\ \varphi_i(\bar{u}_i)^T \\ \dots \\ \varphi_S(\bar{u}_{\bar{Q}})^T \\ \varphi_1(\bar{u}_1)^T \\ \dots \\ \varphi_i(\bar{u}_i)^T \\ \dots \\ \varphi_S(\bar{u}_{\bar{Q}})^T \end{bmatrix} \tag{14}$$

where  $\Theta_l \in R^{S,2 \times S}$  is the diagonal matrix containing the thrust and the torque coefficient vector for the lower rotor ( $\Theta_l = \text{diag}(\theta_{1_l}^f, \dots, \theta_{S_l}^f, \theta_{1_l}^\tau, \dots, \theta_{S_l}^\tau)$ ) and  $\varphi_i(u_i) \in R^{p,1}$  is the regression matrix for the  $i$ -th lower rotor coefficient, which depends on the  $i$ -th upper normalized rotor velocity  $\bar{u}_i$  estimated from Equation (13), and  $\bar{Q}$ , which represents the total number of upper rotors with coaxial interaction ( $\bar{Q} < Q$ ). In Equation (14), the lower rotor velocities represent the unknown quantities and they can be computed by computing the roots of  $Q$  polynomials or order  $M$ . The overall process of computing upper and lower rotor velocities is then summarized in Algorithm 1.

---

**Algorithm 1** Coaxial Control Allocation algorithm

---

- 1: Compute  $f_i^d, \tau_i^d$  from  $\mu$  (Equation (12))
  - 2: **if** motor is *upper rotor* **then**
  - 3: Find rotor velocity by solving Equation (13) for  $u_{u,i}$
  - 4: **else if** motor is *lower rotor* **then**
  - 5: Find corresponding coaxial upper rotor velocity  $u_{u,i}^{\text{coax}}$
  - 6: Evaluate Equation (14) at  $u_{u,i}^{\text{coax}}$  and solve for  $u_{l,i}$
  - 7: **end if**
-

## 5. Control Allocation Experiments

The following section focuses on the evaluation of the proposed control allocation with a coaxial multirotor in simulation and on a real platform. All comparisons have been analyzed regarding tracking errors for position, orientation, thrust, and body torques.

### 5.1. Experimental Setup

A custom coaxial octarotor platform was designed (Figure 6), with a custom-made core and equipped with eight rotors *KDE5215XF-220* with propellers  $18.5'' \times 6.3$  in a coaxial contra-rotating configuration. The rotors were arranged symmetrically, with equal spacing, each positioned at a distance of  $l = 0.25$  m from the drone's Center of Mass, as highlighted in Figure 6. In terms of sensor setup, it was equipped with a *VectorNav VN-100* IMU Sensor and a custom-built autopilot framework. The overall weight of the platform, with batteries, is approximately 20 Kg. The rotor and propeller mounted are the same as the ones used in Section 3 for the model validation.

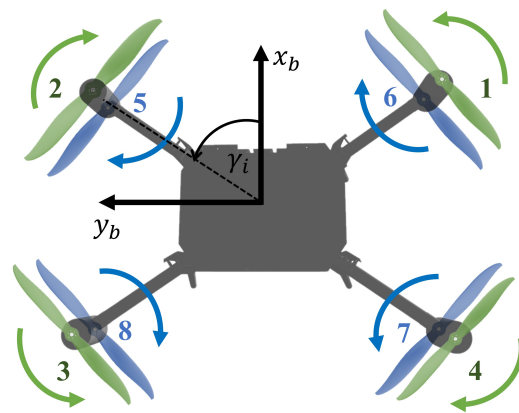


**Figure 6.** Coaxial platform rotor top view highlighting rotor number, rotation sign, and body frames. Upper rotor numbers and rotation signs are highlighted in green, while lower rotor numbers and rotation signs are in blue.

### 5.2. Control Allocation Implementation

This section is devoted to the implementation of the proposed control allocation strategies in the prototype for experiment evaluation in simulation and flight tests.

#### 5.2.1. Reduced Coaxial Mixer

From the geometry of the platform described in Section 5.1 and Equations (6)–(9), the allocation matrix is introduced:

$$A = \begin{bmatrix} 46.98 & 46.98 & 46.98 & 46.98 & 69.89 & 69.89 & 69.89 & 69.89 \\ -8.49 & 8.49 & 8.49 & -8.49 & 12.62 & -12.62 & -12.62 & 12.62 \\ -8.49 & -8.49 & 8.49 & 8.49 & -12.62 & -12.62 & 12.62 & 12.62 \\ -2.44 & 2.44 & -2.44 & 2.44 & -2.00 & 2.00 & -2.00 & 2.00 \end{bmatrix} \quad (15)$$

where the thrust and torque coefficient for upper rotors are equal to  $p_{0,u} = 77.65$  and  $q_{0,u} = 1.93$ , respectively, while lower rotor thrust and torque coefficients are  $p_{0,l} = 69.89$  and  $q_{0,l} = 2.0$ , respectively. Aerodynamic interaction components are equal to  $p_{1,l} = -30.7$  for lower thrust and  $q_{1,l} = -0.5$  for lower torque. The coefficient values adopted in Equation (15) correspond to those identified through the methodology described in Section 3 utilizing LASSO constraint relations, as detailed in Section 3.2. From Equation (15), the normalized rotor velocity vector  $u$  is computed via the Moore–Penrose inverse method  $u = A^+ \mu$  with  $A^+$  the Moore–Penrose inverse matrix of  $A$ , and  $\mu = (f, \tau_x, \tau_y, \tau_z)^T$  the desired forces and momentum vector.

### 5.2.2. Coaxial Mixer

Given the geometry of the platform detailed in Section 5.1, the coaxial mixer of the Equation (9) matrix becomes:

$$A = \begin{bmatrix} 1 & 1 & 1 & 1 & 1 & 1 & 1 & 1 & 0_{1,8} \\ -0.18 & 0.18 & 0.18 & -0.18 & 0.18 & -0.18 & -0.18 & 0.18 & 0_{1,8} \\ -0.18 & -0.18 & 0.18 & 0.18 & -0.18 & -0.18 & 0.18 & 0.18 & 0_{1,8} \\ 0_{1,8} & -1 & 1 & -1 & 1 & -1 & 1 & -1 & 1 \end{bmatrix} \quad (16)$$

where  $A \in R^{4,16}$  is the control allocation matrix. Following the algorithm proposed in Section 4.2, the desired rotor forces and torques are then computed from the Moore–Penrose inverse matrix, as specified in Equation (12). Therefore the relationship between desired forces, torque and rotor velocities for  $i$ -th upper rotor and the corresponding  $j$ -th lower rotor defined in Equation (13) becomes:

$$\begin{bmatrix} f_i^d \\ \tau_i^d \\ f_j^d \\ \tau_j^d \end{bmatrix} = \begin{bmatrix} 55.9517u_i^2 + 22.4464u_i \\ 1.2437u_i^2 + 0.7155u_i \\ (2.755u_i^2 + 64.721)u_j^2 + (12.402 - 2.547u_i)u_j + (0.801 - 37.502u_i^2) \\ (0.307u_i + 1.466)u_j^2 + 0.573u_j - 0.695u_i^2 \end{bmatrix} \quad (17)$$

where the values correspond to the ones identified in Section 3, in particular the ones provided in Table 1, omitting components whose values can be considered negligible. From Equation (16) optimal rotor velocities can be determined using the procedure outlined in Algorithm 1.

### 5.2.3. Standard Mixer

For comparison purposes, a standard mixer has been implemented, based on the platform's geometry. The mixer design follows the approach introduced in [11]. The rotor thrust and torque constants are identified using the rotor testing platform depicted in Figure 1, with the lower rotor removed during the experiments. The identification process relies on the least squares method for the estimation for both the thrust and rotor constants. The resulting identified rotor thrust and torque values are 73.06 N and 1.9 Nm, respectively. Consequently, the standard mixer matrix is derived as follows:

$$A = \begin{bmatrix} 73.06 & 73.06 & 73.06 & 73.06 & 73.06 & 73.06 & 73.06 & 73.06 \\ -13.20 & 13.20 & 13.20 & -13.20 & 13.20 & -13.20 & -13.20 & 13.20 \\ -13.20 & -13.20 & 13.20 & 13.20 & -13.20 & -13.20 & 13.20 & 13.20 \\ -0.026 & 0.026 & -0.026 & 0.026 & -0.026 & 0.026 & -0.026 & 0.026 \end{bmatrix} \quad (18)$$

From Equation (18), the normalized rotor velocities vector is found via the Moore–Penrose inverse method.

### 5.3. Software-In-The-Loop

Before testing on the real platform, a simulator was designed to evaluate the proposed mixers on coaxial platforms. The simulator was developed from [36], with the integration of the coaxial aerodynamic interference (developed in Section 2.1) into the rotor model. To test the simulator with the proposed approaches, the coaxial platform described in Section 5.1 equipped with rotors from Section 3 was integrated into the simulator. As a result, the simulator incorporates the coaxial rotor model of Section 2, developed as a *Gazebo Plugin* and the coaxial mixers developed in Section 4. An IMU sensor and an odometry sensor have been integrated as well as the flight controller proposed in [37]. In order to evaluate the performance of the proposed approach comprehensively, three tests are developed: one employing a standard mixer, one mixer integrating the coaxial rotor model (Algorithm 1), and another one adopting a mixer designed with the reduced coaxial rotor model (Equation (7)). A circular reference has been generated for the three tests, with

a circular trajectory of radius 2 m and a sinusoidal signal for attitude values around 4.5 m after initially hovering at 3 m. All tests were executed utilizing identical controllers and providing the same trajectory to the platform; the only difference is represented by the adopted mixer among the three tests. Data from each experiment were collected through rosbags, including odometry and IMU sensor data, trajectory reference, thrust and torque generated, and rotor speed computed by the chosen mixer. Figure 7 illustrates data from the three experiments. In particular, Figure 7g demonstrates the circular trajectory and the 3D position of the drone for the three tests. The results indicate good tracking performance in the XY plane, as detailed in Figure 7f,e. However, there is a noticeable difference in altitude tracking across the three tests. This discrepancy is more pronounced when observing the attitude tracking error in Figure 7d, in particular with respect to the hovering thrust. This aspect is further evaluated in Table 4 where the average error of pose and control allocation with the different mixers is reported for the tests. The control allocation error mentioned in Table 4 refers to the error between the desired thrust  $f^d$  and torque  $\tau^d$  and the real ones ( $f, \tau$ ):

$$e_f^{ca} = f^d - f, e_\tau^{ca} = \tau^d - \tau \quad (19)$$

Comparing the error in the XY plane in Table 4, the *Reduced-Coaxial Mixer* results in marginally better performance with respect to the other methods for XY position tracking. Although a noticeable improvement is detected in thrust error, where the test with the *Coaxial Mixer* (Figure 7i) achieved an allocation error of 0.58 N, the *Standard Mixer* test shows the worst performance among all mixers with an average of almost 5 N, as also shown in Figure 7i,j. The motivation can be found by comparing the standard rotor model with the model presented in Equation (6). In the latter, the thrust component associated with the upper rotor velocities penalizes the overall thrust of the back rotor. As a result, the control system is unable to maintain a hovering position at 3m during the test, as shown in Figure 7, at approximately 20–25 s. As a consequence, the *Coaxial Mixer* outperforms the *Standard Mixer* and *Reduced-Coaxial Mixer* in terms of attitude tracking for the given tests. *Reduced-Coaxial Mixer* appears to be a good compromise between the two.

**Table 4.** Tracking error and control allocation error in simulation tests using the *Coaxial Mixer*, *Standard Mixer*, and *Reduced-Coaxial Mixer* (R-Coaxial Mixer).

Errors	Control Allocation Method		
	Coaxial Mixer (Section 4.2)	Standard Mixer [5]	R-Coaxial Mixer (Section 4.1)
$e_{p_x}$ [m]	0.3653	0.3656	0.3652
$e_{p_y}$ [m]	0.3662	0.3661	0.3659
$e_{p_z}$ [m]	0.0698	0.6373	0.3335
$e_{\tau_x}^{ca}$ [Nm]	0.10785	0.10451	0.10624
$e_{\tau_y}^{ca}$ [Nm]	0.08570	0.08423	0.0850
$e_{\tau_z}^{ca}$ [Nm]	0.4667	0.00105	0.00108
$e_f^{ca}$ [N]	0.58	4.78	2.75

Further, the behavior of the three mixers for attitude tracking has been analyzed. Yaw error is consistent for the three tests, as illustrated in Figure 7h, although comparing the yaw momentum error in Table 4, *Coaxial mixer* performs worse with respect to the other two. This can be explained by the fact that the *Coaxial Mixer* computes lower rotor velocities, prioritizing rotor thrust tracking with respect to rotor torques, while the *Reduced-Coaxial Mixer* achieves a balance between thrust and torque tracking.

For roll and pitch behavior, the momentum error is analyzed in Table 5: the performance is similar among all the tests.

Overall, the introduced mixers demonstrate the capability to differentiate lower rotor velocities relative to upper rotor velocities (as illustrated in Figure 7a,b), which enables the compensation of thrust and torque loss in lower rotors from the aerodynamic interaction

with upper rotors; in contrast, a state-of-the-art mixer is not capable of differentiating between upper and lower velocities. As a consequence, the two presented mixers generally improve the altitude and attitude tracking of the control system without penalizing its stability.

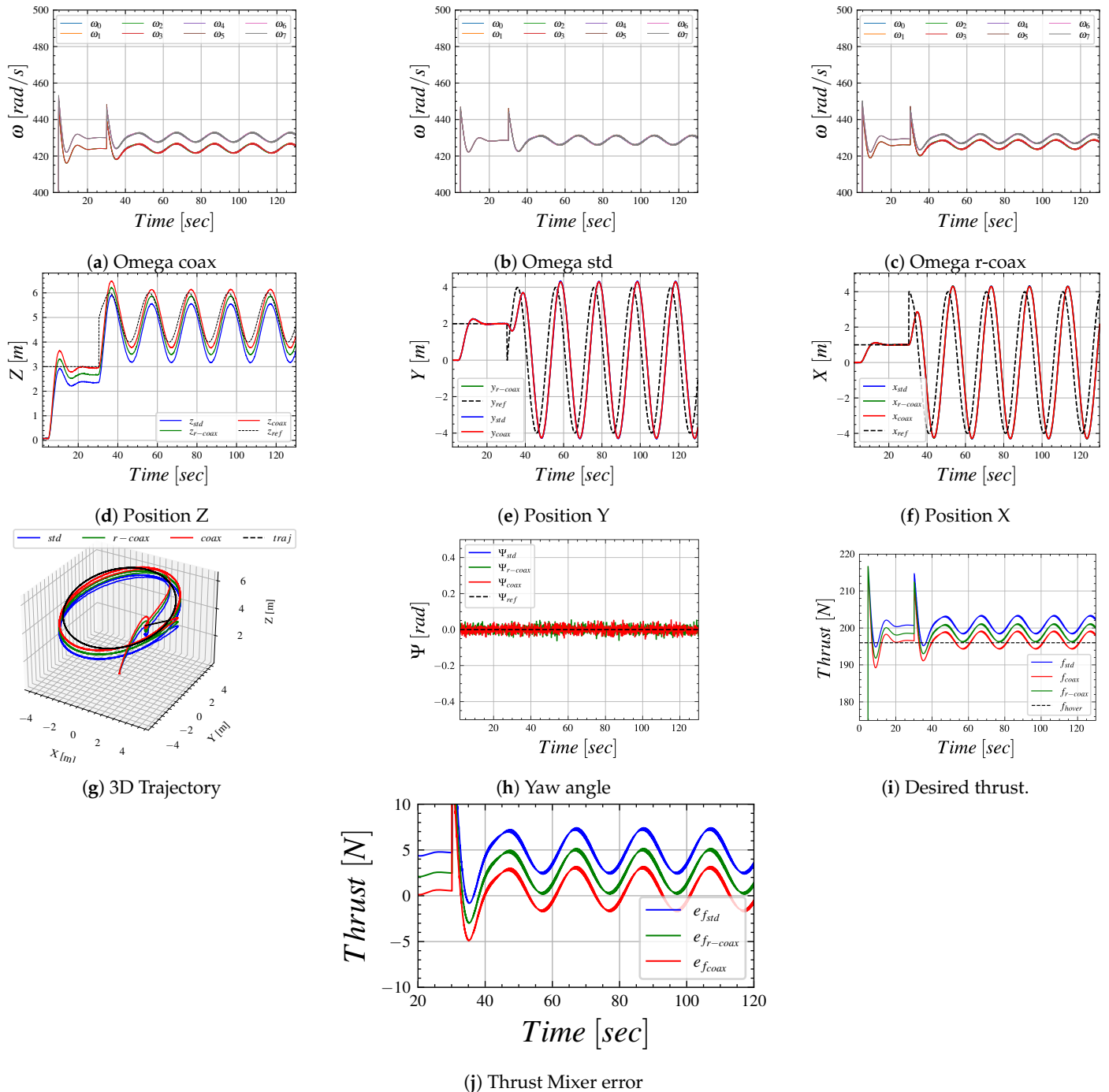


**Figure 7.** Simulation flight test with Coaxial Mixer (coax), Reduce-Coaxial Mixer (r-coax), and with Standard Mixer (std).

#### 5.4. Flight Test

Indoor flight tests have been conducted for the *Standard Mixer* and *Reduced-Coaxial mixer*, which overall appears to decrease allocation error in terms of thrust and torque. Further, due to its structure, it can be easily integrated into a standard mixer structure and it presents low computation consumption with respect to the *Coaxial Mixer*. Both tests

were conducted utilizing the platform of Section 5.1 equipped with the same propellers and motors from Section 3, and the same controller structure and parameters for the two tests (Figure 8). The only variable was the type of mixer. The experiments consisted of two manual flights; in each one, the pilot hovers over the platform to a prescribed altitude and maneuvers it in roll pitch and yaw rate. The results of the experiments are presented in Table 5 and Figure 9.



**Figure 8.** Coaxial platform during indoor tests.

**Table 5.** The table presents the average errors between desired and estimated moments (roll, pitch, yaw) and thrust for both Coaxial and Standard Mixer configurations. The estimated values are derived by applying rotor speeds to the coaxial model outlined in Section 2.

Error Comparison Desired and Estimated Moments and Thrust.		
	Coaxial Mixer (Section 4.2)	Standard Mixer [5]
$e_{xyz}^{ca}$ [Nm]	0.019633, 0.009605, 0.110167	0.141473, 0.076642, 0.3597
$e_f^{ca}$ [N]	11.017573	24.684715

In particular, Table 5 provides the control allocation errors, while Figure 9 illustrates the behavior of the platform during the two tests. The main difference between the two tests is the differentiation of upper and lower rotor velocities in the coaxial mixer, which does not exist in the normal mixer. This differentiation between upper and lower velocities, as a consequence, improves the distribution of forces across the eight rotors, as illustrated in Figure 9e,j, and when the platform hovers for 50, 75, 100 seconds, the *Reduced-Coaxial Mixer* distributes thrust more evenly. In contrast, for tests performed with the *Standard Mixer*, there are observable differences between the upper rotor thrust and the respective lower rotor thrust throughout the entire test, regardless of yaw behavior, as shown in Figure 9j. Consequently, better tracking of the desired thrust torque is achieved in the coaxial test, as evidenced in Table 5, where the *Standard Mixer* achieves an average thrust error of approximately 11.01 N and the coaxial test reaches an average error 24.7N approximately, which seems reasonable with respect to the value found in the experiments in Section 5.3, with a small difference that is due to model error and real flight condition. Regardless of the mixer adopted in the test, in both flights, the platform reaches stable flight conditions in altitude and attitude mode, as shown by the comparison between the reference and the measured roll rate and pitch rate for coaxial and standard tests (respectively, Figure 9b,g). On the other hand, yaw behavior tracking appears to perform with worse tracking performance regardless of the mixer adopted (Figure 9c,h). In particular, it is possible to notice how rotors spinning counterclockwise (rotors 1, 3, 5, and 7) exhibit a higher rotational speed compared to the clockwise-spinning rotors for a standard mixer test



(Figure 9i) and coaxial mixer test (Figure 9d). This is due to the big inertia of the platform due to its size and mass distribution, which makes the control of yaw difficult and requires the pilot to constantly adjust it.

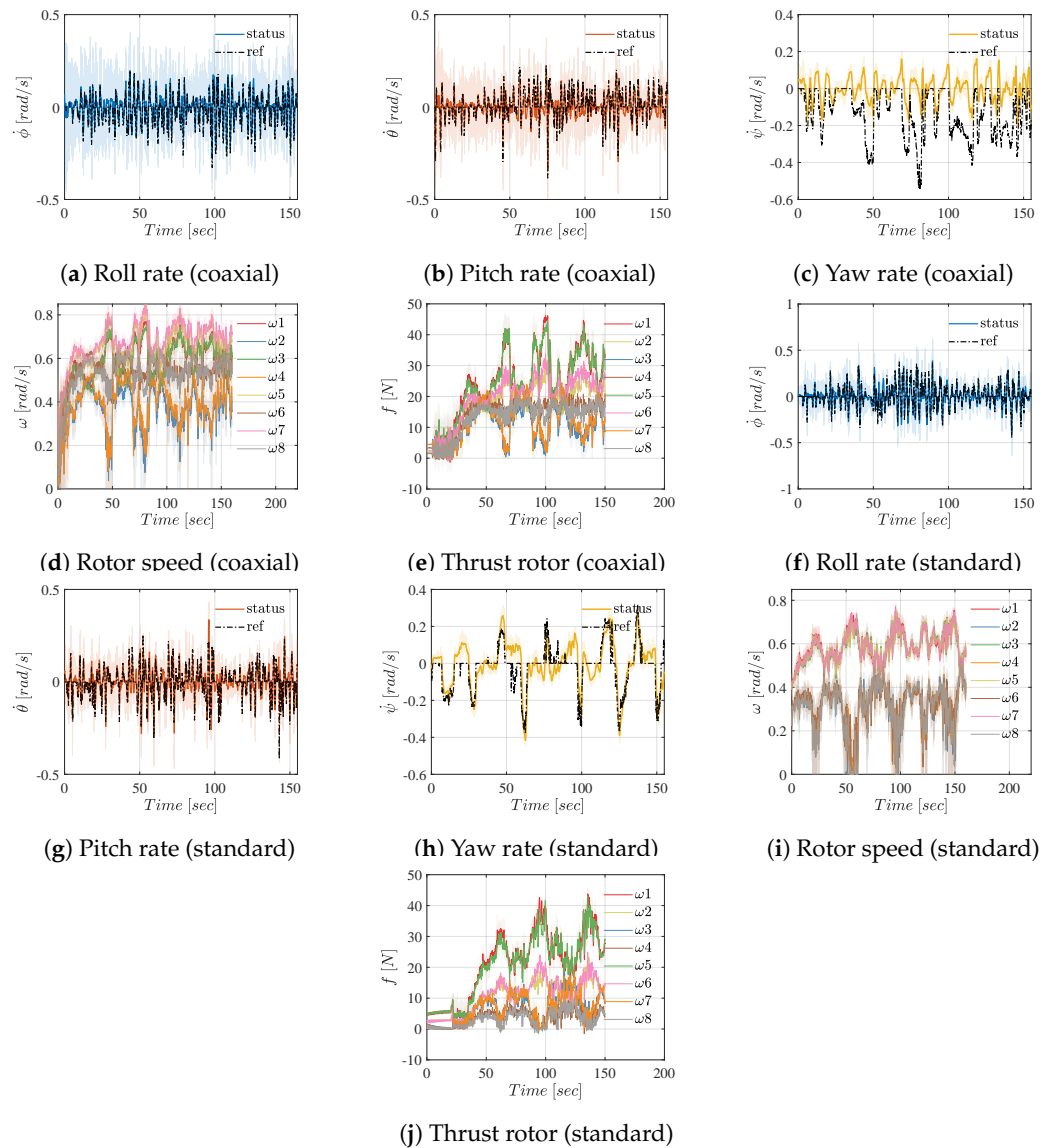


**Figure 9.** Flight test data with standard mixer and coaxial mixer: body rate tracking, desired thrust, desired normalized rotor speed, and estimated rotor thrust.

## 6. Conclusions

This study introduces two novel mixers for coaxial multirotor systems, which offer a significant advancement over the conventional mixer strategy by explicitly incorporating the aerodynamic interactions between coaxial rotors. Key findings include:

- Incorporating aerodynamic interactions into lower rotor models results in a reduction of both thrust and torque errors compared to standard models, with a decrease in thrust error of approximately 12 N and a reduction in total torque error of about 0.043 Nm.
- Adoption of a LASSO-based technique as the identification method for model parameters prevents model overfitting and decreases initial model complexity, thereby improving computational efficiency, with the price of lower accuracy, but still a better one with respect to state-of-the-art solutions. Relaxation of LASSO tolerance results in a further reduction in model complexity, resulting in a quadratic model.

- Two coaxial mixer strategies were implemented based on coaxial rotor models: Coaxial Mixer and Reduced-Coaxial Mixer. The Coaxial Mixer utilizes the pseudo-inversion of a static control allocation matrix, while for Reduced-Coaxial Mixer rotor velocities are derived from the solution of second-order equations. Both mixers improve thrust tracking accuracy and rotor efficiency compared to standard mixer solutions. Specifically:
  - *Coaxial Mixer* generates the minimum thrust and position errors but results in increased attitude error compared to the Reduced-Coaxial Mixer.
  - *Reduced-Coaxial Mixer* achieves better attitude and torque tracking but larger thrust and position errors with respect to the previous one.

Furthermore, the presented works introduce an approach to model coaxial aerodynamic interaction in the rotor model and integrate them in coaxial mixing strategies. Proposed models and mixing strategies have been tested in a real prototype and in simulation. Future work will involve testing the model with various propeller types and coaxial distances, as well as exploring its applicability to multirotors with partial rotor overlap.

**Author Contributions:** Conceptualization, methodology, validation, formal analysis, investigation, resources, writing—original draft, writing—review and editing, A.B.; supervision project administration, M.Á.T.S. and G.H.; funding acquisition, M.Á.T.S. and G.H. All authors have read and agreed to the published version of the manuscript.

**Funding:** The research leading to these results has been supported by AEROTRAIN Marie Skłodowska-Curie (MSCA-ITN-2020-953454) project, funded by the European Commission, by the EAGLE project, funded by the Spanish Ministerio de Ciencia e innovación, Plan de Recuperación, Transformación y Resiliencia, y la Agencia Estatal de Investigación (TED2021-129756B-C32) and by the SIMAR project, funded by the European Union’s Horizon Europe research and innovation programme under grant agreement No. 101070604.

**Data Availability Statement:** Data are contained within the article.

**Conflicts of Interest:** The authors declare no conflicts of interest.

## References

1. Hamandi, M.; Usai, F.; Sablé, Q.; Staub, N.; Tognon, M.; Franchi, A. Design of multirotor aerial vehicles: A taxonomy based on input allocation. *Int. J. Robot. Res.* **2021**, *40*, 1015–1044. [\[CrossRef\]](#)
2. Haddadi, S.J.; Zarafshan, P.; Dehghani, M. A coaxial quadrotor flying robot: Design, analysis and control implementation. *Aerosp. Sci. Technol.* **2022**, *120*, 107260. [\[CrossRef\]](#)
3. Hosseini, S.; Rhein, J.; Sax, F.; Hofstätter, H.; Holzapfel, F.; Maier, L.; Barth, A.; Grebing, B. Conversion of a Coaxial Rotorcraft to a UAV. In Proceedings of the AIAA SciTech 2024 Forum, Orlando, FL, USA, 8–12 January 2024; p. 1716.
4. Marredo, J.; Petrus, A.; Trujillo, M.; Viguria, A.; Ollero, A. A Novel Unmanned Aerial System for Power Line Inspection and Maintenance Operations. In Proceedings of the 2024 International Conference on Unmanned Aircraft Systems (ICUAS), Chania, Greece, 4–7 June 2024; IEEE: Piscataway, NJ, USA, 2024; pp. 602–609.
5. Johansen, T.A.; Fossen, T.I. Control allocation—A survey. *Automatica* **2013**, *49*, 1087–1103. [\[CrossRef\]](#)
6. Monteiro, J.C.; Lizarralde, F.; Hsu, L. Optimal control allocation of quadrotor UAVs subject to actuator constraints. In Proceedings of the 2016 American Control Conference (ACC), Boston, MA, USA, 6–8 July 2016; IEEE: Piscataway, NJ, USA, 2016; pp. 500–505.
7. Faessler, M.; Falanga, D.; Scaramuzza, D. Thrust mixing, saturation, and body-rate control for accurate aggressive quadrotor flight. *IEEE Robot. Autom. Lett.* **2016**, *2*, 476–482. [\[CrossRef\]](#)
8. Johansen, T.A.; Fossen, T.I.; Berge, S.P. Constrained nonlinear control allocation with singularity avoidance using sequential quadratic programming. *IEEE Trans. Control. Syst. Technol.* **2004**, *12*, 211–216. [\[CrossRef\]](#)
9. Bezerra, J.A.; Santos, D.A. Optimal exact control allocation for under-actuated multirotor aerial vehicles. *IEEE Control Syst. Lett.* **2021**, *6*, 1448–1453. [\[CrossRef\]](#)
10. Madruga, S.P.; Tavares, A.H.; Luiz, S.O.; do Nascimento, T.P.; Lima, A.M.N. Aerodynamic effects compensation on multi-rotor UAVs based on a neural network control allocation approach. *IEEE/CAA J. Autom. Sin.* **2021**, *9*, 295–312. [\[CrossRef\]](#)
11. McCormick, B.W. *Aerodynamics, Aeronautics, and Flight Mechanics*; John Wiley & Sons: Hoboken, NJ, USA, 1994.
12. Coleman, C.P. *A Survey of Theoretical and Experimental Coaxial Rotor Aerodynamic Research*; Technical Report; NASA: Washington, DC, USA, 1997.
13. Yoon, S.; Chan, W.M.; Pulliam, T.H. Computations of torque-balanced coaxial rotor flows. In Proceedings of the 55th AIAA Aerospace Sciences Meeting, Grapevine, TX, USA, 9–13 January 2017; p. 0052.
14. Park, S.H.; Kwon, O.J. Numerical study about aerodynamic interaction for coaxial rotor blades. *Int. J. Aeronaut. Space Sci.* **2021**, *22*, 277–286. [\[CrossRef\]](#)

15. Lei, Y.; Wang, J.; Yang, W. Aerodynamic Performance of a Coaxial Hex-Rotor MAV in Hover. *Aerospace* **2021**, *8*, 378. [CrossRef]
16. Khan, H.Z.L.; Mobeen, S.; Rajput, J.; Riaz, J. Nonlinear control allocation: A learning based approach. *arXiv* **2022**, arXiv:2201.06180.
17. Spaans, J.; Gilbert, S.; Stol, K.A.; Al-Zubaidi, S. System Identification for Fully-Actuated UAV Control Allocation. In Proceedings of the 2024 International Conference on Unmanned Aircraft Systems (ICUAS), Nanchang, China, 20–22 September 2024; IEEE: Piscataway, NJ, USA, 2024; pp. 193–200.
18. Malakouti Khah, M.; Esmailifar, S.M.; Saadat, S. Design and development of a novel multirotor configuration with counter-rotating coaxial propellers. *Sci. Rep.* **2024**, *14*, 11580. [CrossRef] [PubMed]
19. Bodie, K.; Taylor, Z.; Kamel, M.; Siegwart, R. Towards efficient full pose omnidirectionality with overactuated mavs. In Proceedings of the 2018 International Symposium on Experimental Robotics, Buenos Aires, Argentina, 5–8 November 2018; Springer: Berlin/Heidelberg, Germany, 2020; pp. 85–95.
20. Dominguez, V.H.; Garcia-Salazar, O.; Amezcua-Brooks, L.; Reyes-Osorio, L.A.; Santana-Delgado, C.; Rojo-Rodriguez, E.G. Micro coaxial drone: Flight dynamics, simulation and ground testing. *Aerospace* **2022**, *9*, 245. [CrossRef]
21. Koehl, A.; Rafaralahy, H.; Boutayeb, M.; Martinez, B. Aerodynamic modelling and experimental identification of a coaxial-rotor UAV. *J. Intell. Robot. Syst.* **2012**, *68*, 53–68. [CrossRef]
22. Chen, L.; Xiao, J.; Zheng, Y.; Alagappan, N.A.; Feroskhan, M. Design, Modeling, and Control of a Coaxial Drone. *IEEE Trans. Robot.* **2024**, *40*, 1650–1663. [CrossRef]
23. Mokhtari, M.R.; Cherki, B.; Braham, A.C. Disturbance observer based hierarchical control of coaxial-rotor UAV. *ISA Trans.* **2017**, *67*, 466–475. [CrossRef]
24. Amado, I. Experimental Comparison of Planar and Coaxial Rotor Configurations in Multi-Rotors. *Instituto Superior Técnico*. **2017**. Available online: <https://api.semanticscholar.org/CorpusID:212412638> (accessed on 13 August 2024).
25. Chen, Z.; Gao, K.; Wang, H.; Wang, L.; Fu, J.; Peng, C. Learning-based modeling and control design for a coaxial helicopter with aerodynamic coupling. *Trans. Inst. Meas. Control.* **2024**. [CrossRef]
26. Prothin, S.; Moschetta, J.M. A Vectoring Thrust Coaxial Rotor for Micro Air Vehicle: Modeling, Design and Analysis. 2013. Available online: <https://core.ac.uk/download/pdf/19892497.pdf> (accessed on 13 August 2024).
27. Chebbi, J.; Defay, F.; Brière, Y.; Deruaz-Pepin, A. Novel model-based control mixing strategy for a coaxial push-pull multirotor. *IEEE Robot. Autom. Lett.* **2020**, *5*, 485–491. [CrossRef]
28. Buzzatto, J.; Liarokapis, M. A benchmarking platform and a control allocation method for improving the efficiency of coaxial rotor systems. *IEEE Robot. Autom. Lett.* **2022**, *7*, 5302–5309. [CrossRef]
29. Ramasamy, M. Hover performance measurements toward understanding aerodynamic interference in coaxial, tandem, and tilt rotors. *J. Am. Helicopter Soc.* **2015**, *60*, 1–17. [CrossRef]
30. Russo, N.; Marano, A.D.; Gagliardi, G.M.; Guida, M.; Polito, T.; Marulo, F. Thrust and Noise Experimental Assessment on Counter-Rotating Coaxial Rotors. *Aerospace* **2023**, *10*, 535. [CrossRef]
31. Lei, Y.; Bai, Y.; Xu, Z.; Gao, Q.; Zhao, C. An experimental investigation on aerodynamic performance of a coaxial rotor system with different rotor spacing and wind speed. *Exp. Therm. Fluid Sci.* **2013**, *44*, 779–785. [CrossRef]
32. Ranstam, J.; Cook, J. LASSO regression. *J. Br. Surg.* **2018**, *105*, 1348. [CrossRef]
33. Tibshirani, R. Regression shrinkage and selection via the lasso. *J. R. Stat. Soc. Ser. B Stat. Methodol.* **1996**, *58*, 267–288. [CrossRef]
34. Plan, Y.; Vershynin, R. The generalized lasso with non-linear observations. *IEEE Trans. Inf. Theory* **2016**, *62*, 1528–1537. [CrossRef]
35. Bangura, M.; Mahony, R. Nonlinear dynamic modeling for high performance control of a quadrotor. In Proceedings of the Australasian Conference on Robotics and Automation, Wellington, New Zealand, 3–5 December 2012.
36. Furrer, F.; Burri, M.; Achtelik, M.; Siegwart, R. Rotors—A modular gazebo mav simulator framework. In *Robot Operating System (ROS) The Complete Reference (Volume 1)*; Springer International Publishing: Cham, Switzerland, 2016; pp. 595–625.
37. Lee, T.; Leok, M.; McClamroch, N.H. Geometric tracking control of a quadrotor UAV on SE(3). In Proceedings of the 49th IEEE Conference on Decision and Control (CDC), Atlanta, GA, USA, 15–17 December 2010; IEEE: Piscataway, NJ, USA, 2010; pp. 5420–5425.

**Disclaimer/Publisher’s Note:** The statements, opinions and data contained in all publications are solely those of the individual author(s) and contributor(s) and not of MDPI and/or the editor(s). MDPI and/or the editor(s) disclaim responsibility for any injury to people or property resulting from any ideas, methods, instructions or products referred to in the content.